

# Slow photoelectron velocity-map imaging spectroscopy of the *n*-methylvinoxide anion

Tara I. Yacovitch,<sup>1</sup> Jongjin B. Kim,<sup>1</sup> Etienne Garand,<sup>1,a)</sup> Derek G. van der Poll,<sup>1,b)</sup> and Daniel M. Neumark<sup>1,2,c)</sup>

<sup>1</sup>Department of Chemistry, University of California, Berkeley, California 94720, USA

<sup>2</sup>Chemical Sciences Division, Lawrence Berkeley National Laboratory, Berkeley, California, 94720, USA

(Received 1 February 2011; accepted 9 March 2011; published online 6 April 2011)

High resolution photoelectron spectra of the *n*-methylvinoxide anion and its deuterated isotopologue are obtained by slow electron velocity-map imaging. Transitions between the  $\tilde{X}^1A'$  anion ground electronic state and the radical  $\tilde{X}^2A''$  and  $\tilde{A}^2A'$  states are observed. The major features in the spectra are attributed to transitions involving the lower energy *cis* conformers of the anion and neutral, while the higher energy *trans* conformers contribute only a single small peak. Franck–Condon simulations of the  $\tilde{X}^2A'' \leftarrow \tilde{X}^1A'$  and  $\tilde{A}^2A' \leftarrow \tilde{X}^1A'$  transitions are performed to assign vibrational structure in the spectrum and to aid in identifying peaks in the *cis*-*n*-methylvinoxy  $\tilde{X}^2A''$  band that occur only through vibronic coupling. The experimental electron affinity and  $\tilde{A}$  state term energy are found to be EA = 1.6106 ± 0.0008 eV and T<sub>0</sub> = 1.167 ± 0.002 eV for *cis*-*n*-methylvinoxy. © 2011 American Institute of Physics. [doi:10.1063/1.3572269]

## I. INTRODUCTION

The spectroscopy and dynamics of reactive free radicals are central to many areas of chemistry. Over the years, negative ion photoelectron spectroscopy, in which a reactive radical can be generated by photodetachment of a mass-selected anion, has developed into a very general and powerful probe of free radicals.<sup>1,2</sup> The capabilities of this type of experiment have been augmented by combining negative ion photodetachment with photoelectron imaging techniques that simultaneously yield photoelectron energy and angular distributions.<sup>3</sup> The slow electron velocity-map imaging (SEVI) method<sup>4</sup> developed in our laboratory is a variant of this type of experiment that yields considerably higher resolution (2–4 cm<sup>-1</sup>) than conventional photoelectron (PE) spectroscopy and fewer experimental challenges than other high-resolution photodetachment techniques,<sup>5</sup> enabling the resolution of low-frequency vibrational modes,<sup>6</sup> spin-orbit fine-structure,<sup>7</sup> and, in favorable cases, effects due to external<sup>8</sup> and internal rotation.<sup>9</sup> Moreover, concurrent determination of the photoelectron angular distribution enables the identification of transitions allowed only through vibronic coupling.<sup>10</sup> In this work, we present the SEVI spectra of the *n*-methylvinoxide anion and examine the effects of multiple isomers and vibronic coupling between close-lying states of the *n*-methylvinoxy radical.

This paper is the third in a series of SEVI studies on the vinoxide and substituted vinoxide anions.<sup>9,11</sup> The corresponding vinoxy-based radicals are intermediates in combustion chemistry,<sup>12,13</sup> as well as in atmospheric reactions such

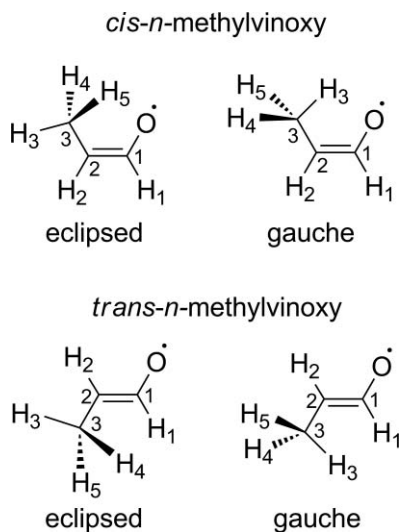
as the tropospheric ozonolysis of alkenes.<sup>14,15</sup> The family of vinyoxy radicals also represents an important model system in electronic spectroscopy, and as such has been investigated extensively in many laboratories.<sup>13,16–26</sup> The SEVI spectra of this series of anions are of particular interest owing to the diversity of spectral phenomena that result from moderate geometry changes upon photodetachment and the presence of different structural isomers. The SEVI spectrum of vinoxide, CH<sub>2</sub>CHO<sup>-</sup>, illustrated Duschinsky mixing of normal modes between the anion and the vinyoxy radical and underlined the importance of including this effect in simulated spectra.<sup>11</sup> Our recent SEVI spectrum of the *i*-methylvinoxide anion revealed fine structure on top of each vibrational transition to the  $\tilde{X}^2A''$  state of the *i*-methylvinoxy radical that was attributed to hindered rotor levels of the methyl substituent accessed upon photodetachment.<sup>9</sup> The subject of this paper, the *n*-methylvinoxy radical, *n*-C<sub>3</sub>H<sub>5</sub>O, (Fig. 1) is a vinyoxy radical with a methyl substituent at the 2-position. It has four possible structural isomers within C<sub>s</sub> symmetry: the *cis* and *trans* isomers, which involve a 180° rotation about the conjugated vinyoxy C(1)–C(2) bond; and the *gauche* and *eclipsed* conformers, which interconvert through rotation of the single bond between C(2) and C(3). The role of these multiple isomers in the spectroscopy of the anion and neutral is of considerable interest.

The *n*-methylvinoxide anion, or propionaldehyde enolate anion, *n*-C<sub>3</sub>H<sub>5</sub>O<sup>-</sup>, is an intermediate in the heterogeneous catalytic oxidation of propanal to acetaldehyde.<sup>27</sup> Similar to the vinoxide and *i*-methylvinoxide enolates, *n*-methylvinoxide is a closed-shell species with an  $\tilde{X}^1A'$  electronic ground state. Photodetachment occurs from the nonbonding π(*a*'') orbital, which is delocalized along the O(1)–C(1)=C(2) vinoxide backbone, to yield the radical  $\tilde{X}^2A''$  state, and from the oxygen lone pair orbital σ<sub>2p</sub>(*a*') to yield the radical  $\tilde{A}^2A'$  state.<sup>28</sup>

<sup>a)</sup>Current address: Department of Chemistry, Yale University, New Haven, Connecticut 06520, USA.

<sup>b)</sup>Current address: Department of Biopharmaceutical Sciences, University of California, San Francisco, California 94143, USA.

<sup>c)</sup>Author to whom correspondence should be addressed. Electronic mail: dneumark@berkeley.edu.

FIG. 1.  $C_s$  isomers of the *n*-methylvinoxy radical.

Extensive photodetachment studies on all methylvinoxide isomers were performed by Brauman and co-workers,<sup>29–31</sup> in which total photodetachment was measured as a function of wavelength. *Cis* and *trans* trimethylsilylated precursors to the *n*-methylvinoxide anions were synthesized, with each yielding a different spectrum. Electron affinities of  $1.73 \pm 0.01$  and  $1.757 \pm 0.033$  eV were reported for *cis*- and *trans*-*n*-methylvinoxy isomers, respectively;<sup>29</sup> these isomer-specific values implicitly assume that no interconversion occurred after ion formation.

The first PE spectra of the *n*-methylvinoxide ions were reported by Ellison *et al.* in 1982.<sup>26</sup> These spectra accessed the  $\tilde{X}^2A' \leftarrow \tilde{X}^1A'$  transition and showed broadened vibronic structure. Alconcel *et al.*<sup>28</sup> later published higher-resolution spectra accessing the  $\tilde{X}$  and  $\tilde{A}$  states of *n*-methylvinoxy. Motivated by previous photodetachment results and simulated spectra, they concluded that the *trans* isomer dominated the spectrum, with a small contribution from *cis*-*n*-methylvinoxy. Extensive laser induced fluorescence (LIF) studies between the radical  $\tilde{X}$  and  $\tilde{B}$  states of the *n*-methylvinoxy radical have been performed by Weisshaar and co-workers.<sup>20,32</sup> The radicals were generated from mixtures of *cis*- and *trans*-ethyl-1-propenyl ether,  $\text{CH}_3\text{CH}=\text{CHOCH}_2\text{CH}_3$ , ranging in composition from 4:1 to 1:4, though the same spectrum was observed for all mixtures. Two backbone vibrations were tentatively identified in the *cis*  $\tilde{B}$  state, and considerable additional structure was attributed to hindered rotation resulting from differing orientations of the methyl group in the  $\tilde{X}$  and  $\tilde{B}$  states.

A number of electronic structure calculations have been performed on this system. Alconcel *et al.*<sup>28</sup> reported energies, geometries, and frequencies for the anion  $\tilde{X}$  state and the radical  $\tilde{X}$  and  $\tilde{A}$  states of *cis*- and *trans*-*n*-methylvinoxy. The *cis* isomer was found to be slightly lower in energy than the *trans* isomer for both the anion (0.080 eV) and neutral (0.03 eV) ground states, in disagreement with their experimental assignment of a primarily *trans* anion photoelectron spectrum. Geometries and energies for the  $\tilde{X}$  and  $\tilde{B}$  states of *cis*- and *trans*-*n*-methylvinoxy radicals were calculated by

Weisshaar and *et al.*,<sup>32</sup> who found the *cis* isomer to be  $\sim 0.020$  eV lower in energy for both states. Their calculations identified the *gauche* orientation (see Fig. 1) of the methyl group as the lower energy conformer for both the *cis* and *trans* isomers of the radical  $\tilde{X}$  state.

In this study, we report high-resolution SEVI spectra of the *n*-methylvinoxide anion and its deuterated isotopologue. We propose a different interpretation of the *n*-methylvinoxide photoelectron spectrum, attributing it almost entirely to transitions between *cis* isomers, with the *trans* isomers contributing only a small origin peak 0.04 eV below the *cis* origin. Franck–Condon (FC) simulations of the  $\tilde{X}^2A' \leftarrow \tilde{X}^1A'$  and  $\tilde{A}^2A' \leftarrow \tilde{X}^1A'$  transitions support this conclusion. Additional peaks in the spectra are attributed to vibronic coupling in which the *cis*-*n*-methylvinoxy  $\tilde{X}^2A'$  state couples to the  $\tilde{A}^2A'$  state. Our reassignment yields new electron affinities and term energies for *n*-methylvinoxy, while the absence of hindered rotor transitions indicates no change in preferred methyl orientation upon photodetachment.

## II. EXPERIMENTAL

SEVI is a high-resolution variant of negative-ion photoelectron spectroscopy and has been described in detail previously.<sup>4,33</sup> Briefly, negative ions are photodetached with a tunable laser, and the slow electrons are selectively detected using a low-voltage extraction velocity-map imaging (VMI) setup.<sup>34</sup> By varying the detachment wavelength, a number of high-resolution scans over limited energy windows are obtained.

*n*- $\text{C}_3\text{H}_5\text{O}^-$  anions were produced from a gas mixture comprising  $\sim 1\%$  propanal and a balance of argon. The deuterated isotopologue was similarly produced using propanal- $\text{d}_6$ , which was synthesized from propanol- $\text{d}_8$  by reaction with pyridinium chlorochromate.<sup>35</sup> The reaction was performed neat to prevent solvent contamination, and vapor from the product mixture was used without further purification.

The gas mixture, at a stagnation pressure of 300 psi, was expanded into the source vacuum chamber through an Even–Lavie pulsed valve.<sup>36</sup> Anions were formed using the grid discharge source described previously.<sup>37</sup> These anions were mass-selected<sup>38</sup> and directed to the detachment region by a series of electrostatic lenses and pinholes. They were then photodetached between the repeller and the extraction plates of the VMI stack by the output of a Nd:YAG pumped tunable dye laser. The resulting photoelectron cloud was coaxially extracted down a 50 cm flight tube and mapped onto a detector comprising a pair of chevron-mounted micro-channel plates coupled to a phosphor screen, as is typically used in photofragment and photoelectron imaging experiments.<sup>3,34,39</sup> Events on the screen were collected by a  $1024 \times 1024$  charge-coupled device (CCD) camera and sent to a computer, where they were summed, quadrant-symmetrized, smoothed, and inverse-Abel transformed.<sup>40</sup> Photoelectron kinetic energy spectra were obtained via angular integration of the transformed images. In each SEVI image, better energy resolution is obtained for slower electrons. Hence, by varying the laser wavelength, a series of spectra is obtained in which different transitions are well-resolved. SEVI spectra are plotted

TABLE I. eBE, frequencies, PAD and assignments for the  $\tilde{X}^2A'' \leftarrow \tilde{X}^1A'$  transition to the ground state *n*-C<sub>3</sub>H<sub>5</sub>O and *n*-C<sub>3</sub>D<sub>5</sub>O radicals.

<i>n</i> -C <sub>3</sub> H <sub>5</sub> O					<i>n</i> -C <sub>3</sub> D <sub>5</sub> O				
eBE (cm <sup>-1</sup> )	Offset <sup>a</sup> (cm <sup>-1</sup> )	PAD <sup>b</sup>	Assignment		eBE (cm <sup>-1</sup> )	Offset <sup>a</sup> (cm <sup>-1</sup> )	PAD <sup>b</sup>	Assignment	
			<i>cis</i> <sup>c</sup>	<i>trans</i>				<i>cis</i> <sup>c</sup>	<i>trans</i>
Z	12661.2	-329		0-0	z	12593.7	-334		0-0
A	12990.2	0	s+d	0-0	a	12927.8	0	s+d	0-0
B	13282.7	293	s+d / p	14 <sub>0</sub> <sup>1</sup> and *20 <sub>0</sub> <sup>1</sup>	b	13174.1	246		14 <sub>0</sub> <sup>1</sup> and *20 <sub>0</sub> <sup>1</sup>
C	13609.8	620	p	*19 <sub>0</sub> <sup>1</sup>	c	13393.9	466	p	*19 <sub>0</sub> <sup>1</sup>
D	13685.4	695	s+d	13 <sub>0</sub> <sup>1</sup>	d	13526.3	599	s+d	13 <sub>0</sub> <sup>1</sup>
E	14151.4	1161	s+d	10 <sub>0</sub> <sup>1</sup>	e	13991.2	1063		9 <sub>0</sub> <sup>1</sup> and *16 <sub>0</sub> <sup>1</sup>
F	14189.1	1199		7 <sub>0</sub> <sup>1</sup> , 8 <sub>0</sub> <sup>1</sup> , 9 <sub>0</sub> <sup>1</sup>	f	14129.3	1202		13 <sub>0</sub> <sup>2</sup>
G	14392.3	1402	p	6 <sub>0</sub> <sup>1</sup> and *16 <sub>0</sub> <sup>1</sup>	g	14262.0	1334	s+d	6 <sub>0</sub> <sup>1</sup>
H	14568.6	1578	s+d	5 <sub>0</sub> <sup>1</sup>	h	14466.9	1539	s+d	5 <sub>0</sub> <sup>1</sup>

<sup>a</sup>Offset indicates distance from major peak A.

<sup>b</sup>Entries are left blank for peaks that are too low in intensity determine a PAD.

<sup>c</sup>Numbering refers to the normal modes described in Table V and asterisks indicate vibronically allowed transitions. See Sec. V A of text.

with respect to electron binding energy (eBE), defined as the difference between the photodetachment photon energy and the measured electron kinetic energy.

The apparatus was calibrated by acquiring SEVI images of atomic O<sup>-</sup>, S<sup>-</sup>, and I<sup>-</sup> at several photon energies. With the 350 V VMI repeller voltage used in this study, a Gaussian peak width ( $w = 2\sigma$ ) of 2.9 cm<sup>-1</sup> was obtained for an iodide peak 22.9 cm<sup>-1</sup> above threshold. Linewidths in the spectra presented here are limited by unresolved rotational structure, and since the origin of an unresolved rotational profile may not be aligned with the observed peak maximum, we report error bars of one Gaussian standard deviation ( $\frac{1}{2} w = \sigma$ ) for all energy determinations.

SEVI also provides information on the photoelectron angular distribution (PAD). For one-photon detachment, the PAD is given by Eq. (1),<sup>41,42</sup>

$$\frac{d\sigma}{d\Omega} = \frac{\sigma_{\text{total}}}{4\pi} \left( 1 + \beta \left( \frac{3}{2} \cos^2(\theta) - \frac{1}{2} \right) \right), \quad (1)$$

where  $\theta$  is the angle between the direction of the photoelectron ejection and the polarization vector of the incident photon. The anisotropy parameter  $\beta$  is sensitive to the shape and symmetry of the molecular orbital from which detachment occurs.  $\beta = 0$  indicates an isotropic PAD, which we call “s-wave” analogously to the atomic case.  $\beta = 2$  corresponds to a p-wave  $\cos^2\theta$  PAD. Finally, perfect interference between s and d-waves results in  $\beta = -1$ , yielding an “s+d-wave” with a  $\sin^2\theta$  PAD. SEVI anisotropies rarely reach the limiting values above, and so peaks with  $\beta < 0.2$  are simply labeled “s+d” and peaks with  $\beta > 1$  are labeled “p.” These upper and lower bounds are approximate, and if two strong neighboring peaks have very different PADs, their anisotropies are labeled differently even if they do not strictly meet these  $\beta$  cutoffs.

### III. RESULTS

SEVI spectra of the  $\tilde{X}^2A'' \leftarrow \tilde{X}^1A'$  and  $\tilde{A}^2A' \leftarrow \tilde{X}^1A'$  anion-to-radical electronic transitions of *n*-methylvinoxy and its fully deuterated isotopologue are presented in Figs. 2 and 3. In both figures, panel (a) corresponds

to *n*-C<sub>3</sub>H<sub>5</sub>O<sup>-</sup> using upper-case letters to label the peaks, while panel (b) corresponds to *n*-C<sub>3</sub>D<sub>5</sub>O<sup>-</sup>, with peaks labeled in lower-case. Note that the letters refer only to the ordering of the peaks and do not imply the same assignment for the two isotopologues. Peak positions, PADs, and assignments (see Sec. V) are summarized in Tables I and II. Low signal-to-noise prevents the determination of PADs for some low-intensity transitions.

SEVI spectra were constructed as follows. Several SEVI scans were taken at progressively lower photon energies in order to achieve high resolution for each peak. At each detachment energy, two or three experimental scans were averaged. These spectra are shown in Figs. 2 and 3. The highest resolu-

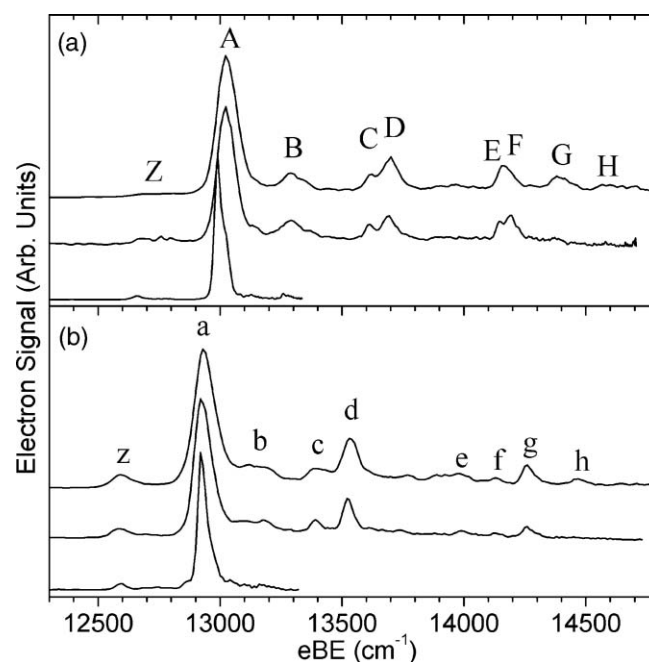


FIG. 2. SEVI spectra of the  $\tilde{X}^2A'' \leftarrow \tilde{X}^1A'$  transition of the *n*-methylvinoxy anion. Panel (a) shows *n*-C<sub>3</sub>H<sub>5</sub>O<sup>-</sup> with traces taken at laser energies of 15 384, 14 706, and 13 351 cm<sup>-1</sup>. Panel (b) shows *n*-C<sub>3</sub>D<sub>5</sub>O<sup>-</sup> with traces taken at laser energies of 15 384, 14 749, and 13 333 cm<sup>-1</sup>.

TABLE II. eBE, frequencies, peak anisotropies, and assignments for the  $\tilde{A}^2A' \leftarrow \tilde{X}^1A'$  transition to the excited state  $n$ -C<sub>3</sub>H<sub>5</sub>O and  $n$ -C<sub>3</sub>D<sub>5</sub>O radicals.

	$n$ -C <sub>3</sub> H <sub>5</sub> O					$n$ -C <sub>3</sub> D <sub>5</sub> O				
	eBE (cm <sup>-1</sup> )	Offset <sup>a</sup> (cm <sup>-1</sup> )	PAD <sup>b</sup>	Assignment		eBE (cm <sup>-1</sup> )	Offset <sup>a</sup> (cm <sup>-1</sup> )	PAD <sup>b</sup>	Assignment	
				<i>cis</i> <sup>c</sup>	<i>trans</i>				<i>cis</i> <sup>c</sup>	<i>trans</i>
I	22074.6	-330	p		0-0	i	21970.3	-336	p	0-0
J	22404.1	0	p		0-0	j	22306.0	0	p	0-0
L	23457.3	1053	p	11 <sub>0</sub> <sup>1</sup> and 10 <sub>0</sub> <sup>1</sup>		l	23100.6	795	p	11 <sub>0</sub> <sup>1</sup>
							23184.7	879		10 <sub>0</sub> <sup>1</sup>
M	23767.2	1363	p	5 <sub>0</sub> <sup>1</sup>		m	23505.2	1199	p	6 <sub>0</sub> <sup>1</sup>
N	24022.1	1618	p	7 <sub>0</sub> <sup>1</sup>		n	23884.8	1579	p	5 <sub>0</sub> <sup>1</sup>

<sup>a</sup>Offset indicates distance from major peak I.<sup>b</sup>Entries are left blank for peaks that are too low in intensity to determine a PAD.<sup>c</sup>Numbering refers to the normal modes described in Table V. See Sec. VB of text.

tion portions of these averages were then spliced together to yield a composite spectrum with high resolution for all peaks, as shown in the top panels of Figs. 4–6. For negative ions, the relative intensity for a given peak decreases with decreasing detachment energy,<sup>43</sup> so each portion of the composite spectrum was also intensity-scaled to match an overview SEVI spectrum taken well above threshold.

Near threshold, the Gaussian width  $w$  of most major peaks is around 25 cm<sup>-1</sup> or more, considerably broader than atomic chloride peaks (4 cm<sup>-1</sup>) obtained under similar conditions. The broader peaks in the molecular SEVI spectra indicate that the experimental resolution is limited by the unresolved asymmetric top rotational envelope and not the instrument.

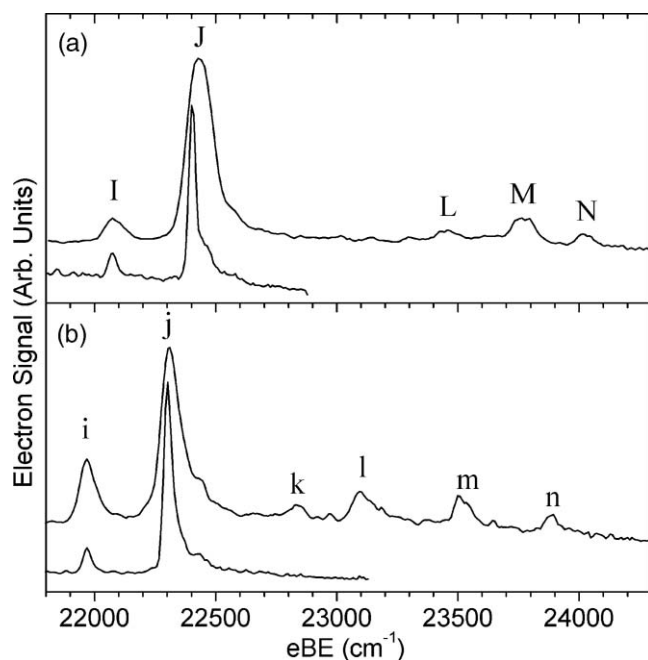


FIG. 3. SEVI spectra of the  $\tilde{A}^2A' \leftarrow \tilde{X}^1A'$  transition of the  $n$ -methylvinoxide anion. Panel (a) shows  $n$ -C<sub>3</sub>H<sub>5</sub>O<sup>-</sup> with traces taken at laser energies of 26 455 and 22 883 cm<sup>-1</sup>. Panel (b) shows  $n$ -C<sub>3</sub>D<sub>5</sub>O<sup>-</sup> with traces taken at laser energies of 24 570 and 23 095 cm<sup>-1</sup>.

The spectra in Figs. 2 and 3 show well-resolved structure dominated by the origin bands (A, a, J, and j), followed by transitions to vibrationally excited levels of the radical  $\tilde{X}$  and  $\tilde{A}$  states. The main additional features of the  $n$ -C<sub>3</sub>H<sub>5</sub>O  $\tilde{X}$  state spectrum [Fig. 2(a)] are peaks B, C, D, E, F, and G, which occur 293, 620, 695, 1161, 1199, and 1402 cm<sup>-1</sup> above the main peak A. The weak peak Z appears 330 cm<sup>-1</sup> below peak A. The deuterated spectrum in Fig. 2(b) shows similar vibrational structure, with frequency shifts for most peaks except peak z. Peak b does not appear in the higher resolution scans shown in Fig. 2(b), but the overview spectrum shows unresolved intensity at this position. The  $\tilde{A}$  state spectrum in Fig. 3(a) is dominated by peak J followed by peaks L, M, and N, lying above peak J by 1053, 1363, and 1618 cm<sup>-1</sup>, respectively. Peak I appears 330 cm<sup>-1</sup> below peak J. The deuterated spectrum in Fig. 3(b) shows similar structure with an additional peak, labeled k, appearing 528 cm<sup>-1</sup> higher in energy than peak j. The spectra in Figs. 2 and 3 show significantly more structure than the previous PE spectra of Ellison *et al.*<sup>26</sup> and Alconcel *et al.*<sup>28</sup>

The most intense peaks (A, a, J, and j) in the  $\tilde{X}$  and  $\tilde{A}$  state spectra (Figs. 2 and 3, respectively) have distinctly different PADs. Most peaks in the  $\tilde{X}$  state spectrum have “s+d” character, while those in the  $\tilde{A}$  state spectrum have “p” character, consistent with assignment of the two bands to transitions to different neutral electronic states. These results provide a means of distinguishing fully allowed features from those allowed only by vibronic coupling. For example, peaks C, c, and G in Fig. 2 have different anisotropy parameters than the surrounding “s+d” peaks (Table I). This is a strong indicator of vibronic coupling between the  $\tilde{X}^2A'$  state and a nearby electronic state with “p” character; the  $\tilde{A}^2A'$  state is an obvious candidate. Several more peaks in the spectra are allowed only through vibronic coupling, as discussed in Secs. V and VI.

## IV. ANALYSIS

### A. Electronic structure calculations

Geometry optimizations and frequency calculations were performed on the ground state of the  $n$ -methylvinoxide anion

TABLE III. Calculated backbone bond lengths ( $r$ ) and angles ( $a$ ) for the *n*-methylvinoxide anion and associated radicals using density functional theory, the B3LYP functional and the 6-311++G\*\* basis set.<sup>a</sup>

	<i>cis</i> - <i>n</i> -methylvinoxy			<i>trans</i> - <i>n</i> -methylvinoxy		
	$\tilde{X}$ anion	$\tilde{X}$ radical	$\tilde{A}$ radical	$\tilde{X}$ anion	$\tilde{X}$ radical	$\tilde{A}$ radical
rC(1)O	1.273	1.235	1.319	1.271	1.235	1.319
rC(1)C(2)	1.383	1.429	1.338	1.381	1.425	1.338
rC(2)C(3)	1.505	1.483	1.502	1.504	1.484	1.502
aOC(1)C(2)	129.7	123.8	129.5	130.7	123.7	129.1
aC(1)C(2)C(3)	122.9	123.2	124.9	123.2	123.8	123.3

<sup>a</sup>Atom labels refer to Fig. 1. Geometries are for the lower energy gauche conformers.

and the  $\tilde{X}$  and  $\tilde{A}$  states of the *n*-methylvinoxy radical. Density functional theory (DFT) was chosen for this study because it balances acceptable accuracy with low computational load. The B3LYP functional was used with the 6-311++G\*\* Pople-style basis set. All frequencies were scaled by a factor of 0.9679 as is standard for B3LYP calculations with Pople-style basis sets.<sup>44</sup> The GAUSSIAN03 suite of programs<sup>45</sup> was used throughout.

The molecular symmetry was restricted to the  $C_s$  point group, consistent with previous studies on the methylvinoxy isomers.<sup>28,32</sup> All of the isomers shown in Fig. 1 were calculated, though only the lowest energy “gauche” isomers were used in subsequent simulations. In this study, we call a conformer “gauche” (or “eclipsed”) when the in-plane methyl hydrogen H(3) is at a 180° (or 0°) dihedral angle from the vicinal hydrogen H(2).

Calculated backbone geometries for the gauche isomers of *cis*- and *trans*-*n*-C<sub>3</sub>H<sub>5</sub>O<sup>-</sup> and *n*-C<sub>3</sub>H<sub>5</sub>O are listed in Table III. Table IV lists energetics calculated here and in previous work. Electron affinities and  $\tilde{A}$  state term energies for both *cis* and *trans* isomers are given, essentially treating them as different molecules, along with *trans-cis* energy differences for the anion and the two neutral states. We find the *cis* isomer to be lower in energy for each all three states. Additionally, in contrast to the *i*-methylvinoxide system where the preferred methyl rotor orientation depends on the electronic state,<sup>9,32</sup> the lowest-energy methyl orientation for *n*-C<sub>3</sub>H<sub>5</sub>O<sup>-</sup> and *n*-C<sub>3</sub>H<sub>5</sub>O is gauche for all computed states.

A crude B3LYP/6-31G\* scan of the interconversion of *cis* and *trans* structures, keeping all other geometries constant, yielded *cis/trans* barrier heights of 20 093 cm<sup>-1</sup> for the anion  $\tilde{X}$  state, 6376 cm<sup>-1</sup> for the radical  $\tilde{X}$  state, and 10 314 cm<sup>-1</sup> for the radical  $\tilde{A}$  state. We estimate the temperature in the supersonic expansion to be around 70 K and thus expect no interconversion of these isomers once they are formed. An experimental value for the *cis*-*n*-methylvinoxy  $\tilde{X}$  state barrier to internal rotation has been determined as 200 ± 20 cm<sup>-1</sup> by fitting LIF hot bands.<sup>32</sup>

Selected scaled frequencies for the *cis* anion and radical and their normal mode descriptions are listed in Table V. Values for the deuterated molecules are also included. These frequencies generally agree with the reported results of Alconcel *et al.*<sup>28</sup> at the CASSCF/6-311++G\*\* level of theory, with differences under 30 cm<sup>-1</sup> for most modes, and larger discrepancies for modes involving methyl CH motions. Normal modes in a 9-atom system such as

*n*-methylvinoxy become quite complicated, so the normal mode descriptions are necessarily simplified. The anion and radical vibrational modes are generally similar, but care was taken to match them according to their greatest overlap (see discussion of the **J** matrix in Sec. IV B). Within each symmetry ( $a'$  or  $a''$ ), the vibrations are ordered according to their calculated frequencies in the  $\tilde{X}$  state of the *n*-C<sub>3</sub>H<sub>5</sub>O radical.

## B. Franck–Condon simulations

Franck–Condon simulations were performed on the  $\tilde{X} \ ^2A'' \leftarrow \tilde{X} \ ^1A'$  and  $\tilde{A} \ ^2A' \leftarrow \tilde{X} \ ^1A'$  transitions using frequencies and geometries from the electronic structure calculations. Line intensities are proportional to Franck–Condon

TABLE IV. Experimental and theoretical adiabatic electron affinities (EA) and term energies ( $T_0$ ), along with theoretical *trans-cis* energy differences ( $E_{trans}-E_{cis}$ ) of *n*-methylvinoxide and *n*-methylvinoxy (in eV).

Expt.	<i>cis</i>	<i>trans</i>	
EA	1.6106 ± 0.0008	1.570 ± 0.002	
EA ( <i>n</i> -C <sub>3</sub> D <sub>5</sub> O)	1.603 ± 0.002	1.561 ± 0.001	
EA <sup>a</sup>	1.76	1.59 ± 0.02	
EA <sup>b</sup>	1.73 ± 0.01	1.619 ± 0.007	
T <sub>0</sub>	1.167 ± 0.002	1.167 ± 0.003	
T <sub>0</sub> ( <i>n</i> -C <sub>3</sub> D <sub>5</sub> O)	1.163 ± 0.003	1.163 ± 0.002	
T <sub>0</sub> <sup>a</sup>	0.99 ± 0.2	1.19 ± 0.02	
Theory <sup>c</sup>	<i>cis</i>	<i>trans</i>	
EA B3LYP <sup>d</sup>	1.551	1.513	
EA CASSCF <sup>a</sup>	-0.05	-0.10	
EA CASSCF-MP2 <sup>a</sup>	1.54	1.49	
T <sub>0</sub> B3LYP <sup>d</sup>	1.160	1.163	
T <sub>0</sub> CASSCF <sup>a</sup>	1.09	1.03	
T <sub>0</sub> CASSCF-MP2 <sup>a</sup>	1.24	1.19	
Theory ( $E_{trans}-E_{cis}$ ) <sup>c,e</sup>	$\tilde{X}$ anion	$\tilde{X}$ radical	$\tilde{A}$ radical
B3LYP <sup>d</sup>	0.062	0.023	0.026
CASSCF <sup>b</sup>	0.069	0.016	-0.037
CASSCF-MP2 <sup>b</sup>	0.082	0.029	-0.028
CASSCF(5,4) <sup>f</sup>		0.02	

<sup>a</sup>Reference 28.

<sup>b</sup>Reference 29.

<sup>c</sup>Calculated values use the indicated method and the 6-311++G\*\* basis set unless otherwise indicated.

<sup>d</sup>B3LYP energies are for the gauche conformers (see Fig. 1).

<sup>e</sup>Positive values indicate a more stable *cis* conformer.

<sup>f</sup>Reference 32 using a 6-31G\*\* basis set.

TABLE V. Selected normal modes and scaled vibrational frequencies of the *cis*-gauche lowest energy isomers of the *cis*-*n*-methylvinoxide anion and *cis*-*n*-methylvinoxy radicals calculated at the B3LYP/6-311++G\*\* level of theory.

Mode	Symmetry	<i>cis</i> - <i>n</i> -C <sub>3</sub> H <sub>5</sub> O			<i>cis</i> - <i>n</i> -C <sub>3</sub> D <sub>5</sub> O			Description <sup>a</sup>
		$\tilde{X}$ anion	$\tilde{X}$ radical	$\tilde{A}$ radical	$\tilde{X}$ anion	$\tilde{X}$ radical	$\tilde{A}$ radical	
5	<i>a'</i>	1391	1519	1321	1522	1487	1560	CO stretch; asymmetric CCO stretch
6	<i>a'</i>	1443	1439	1445	1311	1310	1173	asymmetric CCC stretch; symmetric methyl bend
7	<i>a'</i>	1552	1374	1589	1034	1009	1040	asymmetric CCC stretch; all CH rocks
8	<i>a'</i>	1297	1352	1177	1065	1098	1068	asymmetric CCO stretch; all CH rocks
9	<i>a'</i>	1325	1341	1372	1000	1022	947	all CH rocks
10	<i>a'</i>	1120	1136	1047	915	938	880	asymmetric CCC stretch; CH(2) and CH <sub>3</sub> rocks
11	<i>a'</i>	1024	1034	1007	824	813	789	out-of-phase CH(2) and CH <sub>3</sub> rocks
13	<i>a'</i>	688	674	586	596	588	527	out-of-phase CCO and CCC bends
14	<i>a'</i>	244	260	220	222	237	203	in-phase CCC and CCO bends
16	<i>a''</i>	1435	1425	1437	1038	1028	1035	asymmetric methyl bend
19	<i>a''</i>	601	631	711	453	476	559	CH(2) wag
20	<i>a''</i>	342	294	427	288	244	362	backbone wag
21	<i>a''</i>	70	102	108	51	74	78	methyl torsion

<sup>a</sup>Mode descriptions refer to the  $\tilde{X}$  state radical for *cis*-*n*-C<sub>3</sub>H<sub>5</sub>O in the gauche methyl configuration (see Fig. 1).

factors (FC) between the wavefunctions  $\psi_v^i$  and  $\psi_{v'}^f$  for the anion and neutral vibrational levels, respectively:

$$FC = \left| \int \psi_{v'}^{*f} \cdot \psi_v^i d\tau \right|^2. \quad (2)$$

The Born–Oppenheimer approximation is assumed, as well as a constant electronic transition moment. For multidimensional systems (*n*-methylvinoxy has 21 normal modes), *v* and *v'* each correspond to a set of vibrational quantum numbers for the anion and radical, respectively. The initial (**Q**) and final (**Q'**) normal coordinates are related by the Duschinsky transformation,<sup>46</sup>

$$\mathbf{Q} = \mathbf{J}\mathbf{Q}' + \mathbf{K}. \quad (3)$$

Here, **J** is the Duschinsky rotation matrix which represents the mixing of normal modes. **K** is the normal coordinate displacement vector that expresses the difference between the neutral and anion equilibrium geometries in terms of the neutral normal coordinates.

Using the set of programs prepared by Ervin and co-workers, the **J** matrix and **K** vector for all vibrations are computed in FCFGAUS,<sup>47</sup> and then all modes are treated with Duschinsky rotation in PESCAL.<sup>48</sup> The normal modes between initial and final states are matched such that the **J** matrix is a diagonal as possible, though significant off-diagonal mixing occurs for the backbone stretching modes, especially in the *n*-C<sub>3</sub>H<sub>5</sub>O<sup>−</sup> simulations: modes  $\nu_5$ ,  $\nu_6$ , and  $\nu_7$  are mixed in the  $\tilde{X} \leftarrow \tilde{X}$  simulation, and modes  $\nu_5$ ,  $\nu_7$ ,  $\nu_8$ ,  $\nu_{10}$ , and  $\nu_{11}$  are mixed in the  $\tilde{A} \leftarrow \tilde{X}$  simulation. Alternate mode matching schemes would yield the same spectrum, merely affecting the labeling of some peaks.

Our previous study of *i*-C<sub>3</sub>H<sub>5</sub>O showed that the  $\nu_{21}$  mode corresponding to methyl rotation was better represented as a hindered rotor rather than a vibrational mode.<sup>9</sup> Hence, we leave out the  $\nu_{21}$  mode in the *n*-methylvinoxy FC simulations. In any case, we do not expect hindered rotor activity here since the methyl group orientation does not change between the initial anion and final radical states.

## V. ASSIGNMENT

Figure 4 compares experimental spectra for the  $\tilde{X}$  and  $\tilde{A}$  bands (top panels) to the results of *cis*←*cis* and *trans*←*trans* FC simulations (middle and bottom panels). Lining up the simulated 0–0 transitions with the dominant peak in all spectra, the *cis* simulations largely reproduce the experimental intensities, leaving only a few experimental peaks unaccounted for. The *trans* simulations do not fit nearly as well, showing considerably more vibrational activity in the  $\tilde{X}$  band than is seen experimentally. It thus appears that the spectra of *n*-methylvinoxide are dominated by the *cis*-*n*-methylvinoxy isomer. This conclusion is consistent with the calculated *trans*-*cis* energy differences shown in Table IV in which the *cis*-*n*-methylvinoxide anion is at least 0.06 eV more stable than the *trans* anion. From the

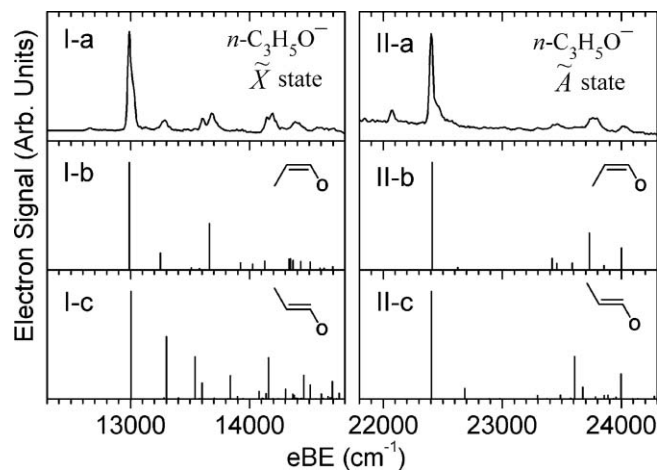


FIG. 4. Comparison of FC simulations for *cis*- and *trans*-*n*-C<sub>3</sub>H<sub>5</sub>O<sup>−</sup>. The left panels show the ground  $\tilde{X}$  state and the right panels show the excited  $\tilde{A}$  state. Panel (a) shows composite experimental spectra. Panels (b) and (c) show simulated line spectra for *cis*- and *trans*-*n*-methylvinoxide, respectively, with geometries and frequencies calculated at the B3LYP/6-311++G\*\* level of theory. The origins of the simulated spectra are aligned with the most intense experimental peaks.

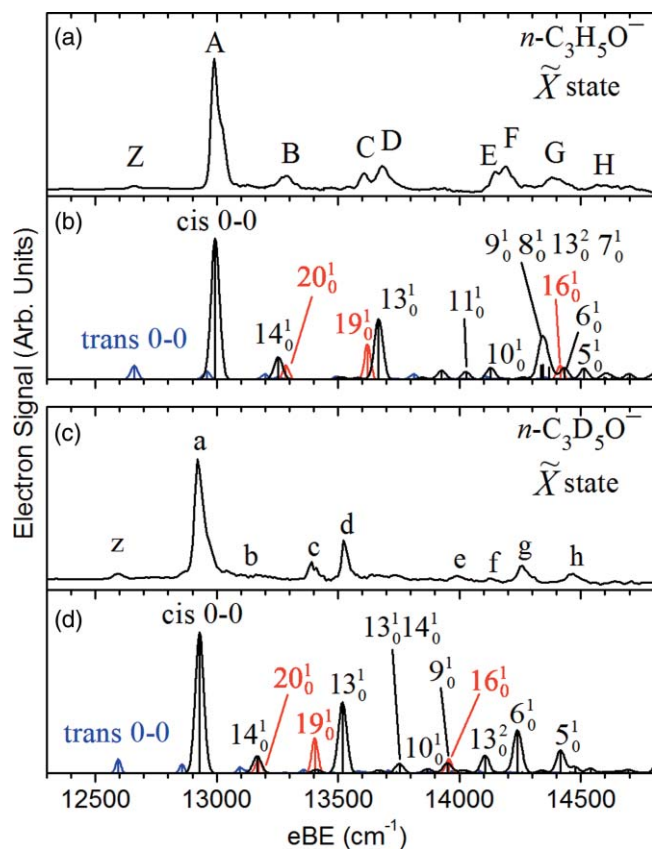


FIG. 5. The  $\tilde{X} \ ^2A'' \leftarrow \tilde{X} \ ^1A'$  transition of *n*-methylvinoxide. Panels (a) and (c) show composite experimental traces of  $n\text{-C}_3\text{H}_5\text{O}^-$  and  $n\text{-C}_3\text{D}_5\text{O}^-$ , respectively. The composite spectrum is made by joining parts of spectra acquired at laser energies above threshold by 2394, 1216, 1357, 1154, and 361  $\text{cm}^{-1}$  in panel (a) and 2457, 1821, 856, and 406  $\text{cm}^{-1}$  in panel (c). Panels (b) and (d) show the associated simulated FC spectra of gauche *cis*-*n*-methylvinoxide in black and *trans*-*n*-methylvinoxide in blue. The origins are matched to experimental peak positions and the relative intensities are 10:1 *cis:trans*. In red, nominally forbidden transitions in nontotally symmetric modes of *cis*-*n*-methylvinoxy are also shown, with frequencies as calculated and intensities matched to experiment. Gaussian convolutions of line spectra are shown with a width  $w = 25 \text{ cm}^{-1}$ .

comparison in Fig. 4 alone, it is not clear if the entire SEVI spectrum can be attributed to the *cis* isomer, or if some *trans* contribution is needed to fit the missing peaks in the *cis* simulations. In the remainder of this section, we will show that all features in the SEVI spectra can be assigned exclusively to the *cis* isomer, with the exception of the small peak below each *cis*-*n*-methylvinoxide origin. All other peaks that are missing from the *cis* FC simulations can be attributed to nominally forbidden transitions that are allowed only by vibronic coupling.

Figures 5 and 6 present a more detailed comparison of the experimental results with *cis*←*cis* simulations. Assignments indicated in the simulated spectra are discussed in detail in the remainder of this section. As discussed more fully below, the black traces in the simulated spectra are fully FC allowed transitions of the *cis* isomer, while the red traces indicate *cis* isomer transitions allowed only through vibronic coupling. The blue traces correspond to *trans*←*trans* simulations, with only the origin transition appearing with significant intensity. Results from Figs. 5 and 6 were used

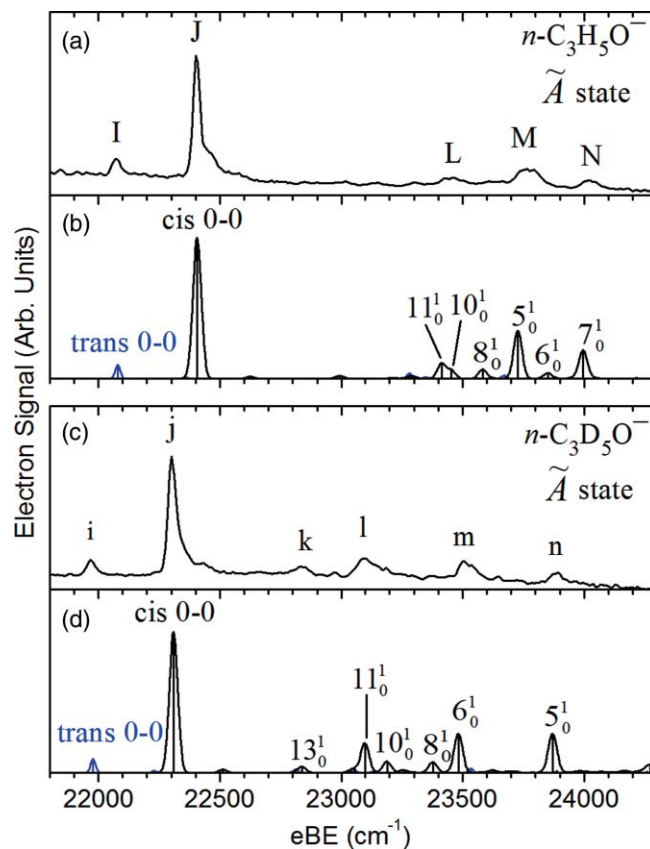


FIG. 6. The  $\tilde{A} \ ^2A' \leftarrow \tilde{X} \ ^1A'$  transition of *n*-methylvinoxide. Panels (a) and (c) show composite experimental traces of  $n\text{-C}_3\text{H}_5\text{O}^-$  and  $n\text{-C}_3\text{D}_5\text{O}^-$ , respectively. The composite spectrum is made by joining parts of spectra acquired at laser energies above threshold by 4051 and 479  $\text{cm}^{-1}$  in panel (a); 2264 and 789  $\text{cm}^{-1}$  in panel (c). Panels (b) and (d) show the associated simulated FC spectra of gauche *cis*-*n*-methylvinoxide in black and *trans*-*n*-methylvinoxide in blue. The origins are matched to experimental peak positions and the relative intensities are 10:1 *cis:trans*. Gaussian convolutions of line spectra are shown with a width  $w = 25 \text{ cm}^{-1}$ .

to make the assignments discussed below and reported in Tables I and II.

### A. $\tilde{X}$ state

We begin by assigning those peaks in Fig. 5 that are fully allowed without invoking any inter-state vibronic coupling. The  $\tilde{X}$  state spectrum is dominated by peak A in  $n\text{-C}_3\text{H}_5\text{O}^-$  and peak a in  $n\text{-C}_3\text{D}_5\text{O}^-$ . We assign these intense features to the vibrational origin transitions of *cis*-*n*-methylvinoxide. Previous photoelectron spectroscopy results assigned these transitions to the other isomer, *trans*-*n*-methylvinoxide.<sup>28</sup>

Peaks D and d occur 695 and 599  $\text{cm}^{-1}$  above the origin bands in  $n\text{-C}_3\text{H}_5\text{O}^-$  and  $n\text{-C}_3\text{D}_5\text{O}^-$ , respectively. We assign them to the  $13_0^1$  transition in the CCO bending mode, for which the calculated frequencies in Table I are 674 and 588  $\text{cm}^{-1}$ ; no other totally symmetric mode has a calculated frequency in this range. This mode also contains significant CCC bending character (out-of-phase with the CCO bend), though mostly in the  $n\text{-C}_3\text{H}_5\text{O}$  isotopologue.

The next few peaks are straightforwardly assigned in the  $n\text{-C}_3\text{D}_5\text{O}^-$  spectrum [Fig. 5(c)]. Peak e at 1063  $\text{cm}^{-1}$

corresponds to the  $9_0^1$  transition of the  $\nu_9$  rocking mode of all CD bonds calculated at  $1022\text{ cm}^{-1}$ , though as discussed later, it may also contain contributions from a transition allowed only through vibronic coupling. Peaks f and g are also directly assigned based on FC simulations: peak f at  $1202\text{ cm}^{-1}$  is the  $13_0^2$  transition in the CCO bending mode and peak g at  $1334\text{ cm}^{-1}$  is the  $6_0^1$  transition in the CCC asymmetric stretch; the calculated harmonic values are  $1176$  and  $1310\text{ cm}^{-1}$ , respectively. As expected, peak g has definite “s+d” anisotropy, though peaks e and f are too weak to determine an anisotropy parameter.

Assignments in the analogous region of the  $n\text{-C}_3\text{H}_5\text{O}^-$  spectrum are somewhat different. Peak E at  $1161\text{ cm}^{-1}$  is closest to the simulated  $10_0^1$  transition, a CCC asymmetric stretching mode with a calculated harmonic frequency of  $1136\text{ cm}^{-1}$ . Peak F, which lies  $1199\text{ cm}^{-1}$  from the origin, does not correspond to the  $6_0^1$  transition; this transition is calculated to appear with low intensity underneath peak G ( $6_0^1$  at  $1439\text{ cm}^{-1}$ ). Instead, the *cis* FC simulations predict a strong peak at  $1355\text{ cm}^{-1}$  from the origin due to a sum of 4 allowed transitions:  $7_0^1$ ,  $8_0^1$ ,  $9_0^1$ , and  $13_0^2$ . We propose a tentative assignment of peak F as a sum of peaks  $7_0^1$ ,  $8_0^1$ ,  $9_0^1$ , under the assumption that their calculated harmonic frequencies overestimate the true frequencies. Modes  $\nu_7$ ,  $\nu_8$ , and  $\nu_9$  all contain significant CH rocking motions, including rocking of the methyl hydrogens, whereas  $\nu_{13}$  is primarily a backbone mode. The calculated harmonic frequencies assume a rigid equilibrium structure (no internal methyl rotation). As a consequence, the frequencies for  $\nu_7$ ,  $\nu_8$ , and  $\nu_9$  might not be especially accurate when describing normal modes involving the methyl moiety, which undergoes hindered rotation as in the *i*-methylvinoxide system. Together, peaks E and F in the  $n\text{-C}_3\text{H}_5\text{O}$  spectrum are “s+d,” so we have not attributed them to transitions that might be allowed only through vibronic coupling with another electronic state. However, they are too close together to individually resolve their anisotropies, and we do not rule out some vibronic contribution to their intensities.

FC simulations of the region around the broad peaks H and h predict a transition in the  $\nu_5$  mode as well as a number of low-intensity combination bands, such as the  $13_0^1 11_0^1$  and  $14_0^1 8_0^1$  transitions. We do not observe an isotope shift for the onset of peaks H and h, but we do observe a narrowing of the high-energy tail with deuteration. We thus assign the onset of peaks H and h to the  $5_0^1$  backbone transition and the high energy tail to the overlapping  $13_0^1 11_0^1$  and  $14_0^1 8_0^1$  combination bands. In both Figs. 5 and 6, the simulated  $\nu_5$  frequency is too low by approximately  $59\text{ cm}^{-1}$  (for peak H) and  $54\text{ cm}^{-1}$  (for peak h), an indication that the CO bond is weaker and has less double-bond character than simulated.

Several peaks in the experimental spectra in Fig. 5 do not appear in the FC simulations. Many of these exhibit “p-wave” PADs, suggesting they are nominally forbidden transitions involving  $a''$  vibrational modes that become allowed through vibronic (Herzberg–Teller) coupling with the nearby  $\tilde{A}^2 A'$  state of the radical. The effects of this type of vibronic coupling on PADs in photoelectron spectroscopy are well-documented.<sup>49,50</sup> The intensities of such transitions are not entirely straightforward to calculate, but the peak positions

can be compared to the calculated frequencies for the various  $a''$  vibrational modes. Vibronically allowed transitions that match experimental features are added to the FC simulations as red traces in Figs. 5(b) and 5(d) with intensities scaled to fit the experiment.

Peaks C and c have strong “p” character and are assigned to vibronically allowed transitions on this basis. They occur  $620$  and  $466\text{ cm}^{-1}$  above the origin bands in  $n\text{-C}_3\text{H}_5\text{O}^-$  and  $n\text{-C}_3\text{D}_5\text{O}^-$ , respectively, and are assigned to the  $19_0^1$  transition, an  $a''$  out-of-plane wagging mode of the CH(2) bond. The calculated frequencies of the  $\nu_{19}$  vibration are  $631\text{ cm}^{-1}$  in  $n\text{-C}_3\text{H}_5\text{O}$  and  $475\text{ cm}^{-1}$  in  $n\text{-C}_3\text{D}_5\text{O}$ , very close to the observed values.

Peak G in the  $n\text{-C}_3\text{H}_5\text{O}$  spectrum and, to a lesser degree of certainty, peak e in the  $n\text{-C}_3\text{D}_5\text{O}$  spectrum have “p” anisotropies. The  $\nu_{16}$  mode, an  $a''$  methyl bending vibration, is calculated to have a frequency of  $1425\text{ cm}^{-1}$  in the  $n\text{-C}_3\text{H}_5\text{O}$  radical and  $1028\text{ cm}^{-1}$  in the  $n\text{-C}_3\text{D}_5\text{O}$  radical. These frequencies are close to the positions of peaks G and e at  $1402$  and  $1063\text{ cm}^{-1}$ , respectively. The breadth of peak G can be explained by overlap with the fully allowed  $6_0^1$  transition which is simulated to appear in the tail of peak G.

Peaks B and b at  $293$  and  $246\text{ cm}^{-1}$  match the simulated intensities and frequencies of the  $14_0^1$  transition, a fully allowed  $a'$  CCC bending mode. However, in the  $n\text{-C}_3\text{H}_5\text{O}$  spectrum [Fig. 5(a)], peak B has “p” anisotropy. Unfortunately, peak b is too weak in high resolution scans to measure an anisotropy parameter, though it appears with more intensity in lower resolution scans, a possible manifestation of the anion Wigner threshold law for “p-wave” detachment.<sup>45</sup> The out-of-plane  $\nu_{20}$  vibration in  $\tilde{X}^2 A''$   $n\text{-C}_3\text{H}_5\text{O}$  is calculated to have a frequency of  $294\text{ cm}^{-1}$  ( $244\text{ cm}^{-1}$  for  $n\text{-C}_3\text{D}_5\text{O}$ ); this transition could become allowed when the  $\tilde{X}^2 A''$   $\nu_{20}$  ( $a''$ ) vibronic state couples with one of the many  $\tilde{A}^2 A'$  ( $a'$ ) states available. Peaks B and b can thus be attributed to the  $14_0^1$  transition as well as the vibronically allowed  $20_0^1$  transition.

Finally, peaks Z and z occur  $329$  and  $334\text{ cm}^{-1}$  below the origins in the  $n\text{-C}_3\text{H}_5\text{O}$  and  $n\text{-C}_3\text{D}_5\text{O}$  spectra, respectively. These peaks are too weak for a PAD determination. The position of peak Z might suggest assigning it to the  $20_0^1$  hot band of the  $a''$  backbone wag, a vibronically allowed transition which is calculated to have a frequency of  $342\text{ cm}^{-1}$  in the *cis*- $n\text{-C}_3\text{H}_5\text{O}^-$  anion. However, there is almost no isotope shift upon deuteration, whereas the calculated frequency is  $288\text{ cm}^{-1}$  in *cis*- $n\text{-C}_3\text{D}_5\text{O}^-$ . Instead, we assign peaks Z and z to the SEVI origin transitions of *trans*- $n\text{-C}_3\text{H}_5\text{O}^-$  and *trans*- $n\text{-C}_3\text{D}_5\text{O}^-$ , respectively. Such an assignment is consistent with the calculated relative stabilities of the *cis* and *trans* anion isomers at the B3LYP, CASSCF, and CASPT2 levels of theory, which find the *cis* anion more stable in all cases (see Table IV and Ref. 28), explaining its dominance in the spectrum. Our calculated B3LYP energies also predict a *trans*-*n*-methylvinoxy radical EA  $306\text{ cm}^{-1}$  lower than that of *cis*-*n*-methylvinoxy. This difference is very close to the energy gap between peaks Z and A (also z and a) in the SEVI spectra, supporting our assignment of peaks Z and z to the *trans* vibrational origin. Based on these assignments, we determine

new electron affinities for *cis*- and *trans*-*n*-methylvinoxy, as reported in Table IV.

## B. $\tilde{A}$ state

We again start by assigning the fully allowed peaks in Fig. 6. Peaks J and j dominate the  $\tilde{A}$  state spectra. They are assigned to the origin transitions of *cis*-*n*-methylvinoxide based on the overall agreement of the FC simulations. This transition was previously assigned to the other isomer,<sup>28,29</sup> *trans*-*n*-methylvinoxy.

Peak k only appears in the deuterated spectrum [Fig. 6(b)], at a frequency of 528 cm<sup>-1</sup>. By comparing with simulation, we assign it to the 13<sub>0</sub><sup>1</sup> transition of the CCO bending mode, for which the calculated harmonic frequency is 527 cm<sup>-1</sup>. In the deuterated species, this vibration also includes rocking motion of the methyl group. There is some structure in the baseline of the *n*-C<sub>3</sub>H<sub>5</sub>O spectrum [Fig. 6(a)] at around 23 000 cm<sup>-1</sup>, which would give a hydrogen isotope  $\nu_{13}$  frequency of around 612 cm<sup>-1</sup>, but the signal is too low to make a definitive assignment.

Peaks L, M, and N (l, m, and n) show up in both spectra, but are not assigned to the same set of transitions. Comparison with FC simulations allows assignment of peaks L, M, and N to the 11<sub>0</sub><sup>1</sup>, 5<sub>0</sub><sup>1</sup>, and 7<sub>0</sub><sup>1</sup> transitions, while peaks l, m, and n are assigned to 11<sub>0</sub><sup>1</sup>, 6<sub>0</sub><sup>1</sup> and 5<sub>0</sub><sup>1</sup>, respectively. The  $\nu_{11}$  mode is a CH(2) and CH<sub>3</sub> rocking mode which also contains some CO stretching in the  $\tilde{A}$  state, while the other modes are primarily backbone stretching modes (See Table V). It is worth noting that these modes show significant off-diagonal values in the **J** matrix, indicating strong Duschinsky mixing between them and making labeling of the transitions somewhat arbitrary—each of these peaks only contains a majority of the transition indicated. Close examination of peak l in the deuterated spectrum reveals a significant tail, which we attribute to the 10<sub>0</sub><sup>1</sup> transition, a backbone stretching and CH wagging mode. Simulations also predict a 10<sub>0</sub><sup>1</sup> transition for *n*-C<sub>3</sub>H<sub>5</sub>O but it is too close to the 11<sub>0</sub><sup>1</sup> transition to resolve.

The only peaks in Fig. 6 that cannot be assigned to the *cis*-*n*-C<sub>3</sub>H<sub>5</sub>O<sup>-</sup> species are Peaks I and i, which occur 330 and 336 cm<sup>-1</sup> below peak J and j in the *n*-C<sub>3</sub>H<sub>5</sub>O and *n*-C<sub>3</sub>D<sub>5</sub>O spectra, respectively. These peaks occur at almost exactly the same relative position as peaks Z and z in the  $\tilde{X}$  state spectrum and are similarly assigned to the vibrational origin of *trans*-*n*-C<sub>3</sub>H<sub>5</sub>O<sup>-</sup> and C<sub>3</sub>D<sub>5</sub>O<sup>-</sup>. In this case, however, peaks I and i are intense enough to measure a “p” anisotropy, stronger even than that of peak J. This PAD is inconsistent with the alternate assignment of these peaks to the 20<sub>0</sub><sup>1</sup> hot band transitions, which are allowed only through vibronic coupling with the radical  $\tilde{X}$  state and would thus be expected to have PAD’s characteristic of “s+d-wave” detachment. Based on these assignments, we determine new term energies for *cis*- and *trans*-*n*-methylvinoxy, as reported in Table IV.

## VI. DISCUSSION

In Sec. V, we have proposed a new interpretation of the *n*-methylvinoxy photodetachment spectrum: we have shown

that the *cis* isomer can explain nearly the entire SEVI spectrum assuming the presence of vibronic coupling. The only peaks attributed to photodetachment from the *trans* anion are the minor peaks Z, z, I, and i below the vibrational band origins. According to our assignments, the EA of the *trans* isomer is lower by 329 cm<sup>-1</sup> than the *cis* EA. The lower *trans* EA and the dominance of the *cis* isomer in the SEVI spectra are consistent with the calculated energetics in Table IV, which show the *cis* anion to lie at least 0.06 eV below the *trans* anion. However, this ordering of the EA’s and our overall interpretation disagrees with the previous conclusions of Römer *et al.*<sup>29</sup> and Alconcel *et al.*<sup>28</sup>

In the work by Römer *et al.*,<sup>29</sup> total photodetachment cross sections were measured for *n*-methylvinoxide anions generated from the ion-molecule reaction of F<sup>-</sup> with either (E)- or (Z)- trimethylsilyl enol ether, with the goal of producing pure anion stereoisomers and obtaining spectra for each. The photodetachment spectra indeed depend on which precursor was used. The spectrum attributed to the *cis* anion was dominated by direct photodetachment, while that for the *trans* anion showed distinct resonances assigned to dipole-bound anion excited states above the detachment threshold; the presence of such states is consistent with the significantly higher dipole moment expected for the neutral core of the *trans* isomer. They assigned the EA of the *trans* isomer to a resonance in the “*trans*” spectrum at 1.619 eV (766 nm), while a steep increase in the “*cis*” cross section at 1.73 eV (717 nm) was assigned to the EA of the *cis* isomer. Their *cis* EA is higher than their *trans* value, in contrast to our assignment. However, in their “*cis*” spectrum, considerable signal was seen at photon energies below their assigned value of the *cis* EA; this signal was attributed to contamination from the *trans* anion produced by *cis*→*trans* isomerization during or after the ion-molecule reaction used to produce the anions. This process seems unlikely, given that all calculations performed thus far find the *cis* anion to be lower in energy. It seems reasonable to attribute the lower energy detachment signal in their “*cis*” spectrum to the *cis* anion, which would then yield a lower EA. There is in fact a reasonably steep increase in the *cis* detachment cross section around 767–768 nm that corresponds to an EA very close to the *cis* EA obtained from the SEVI spectrum.

Motivated in part by the work by Römer *et al.*, Alconcel *et al.* assigned the most intense peaks in the  $\tilde{X}$  and  $\tilde{A}$  spectra to the 0–0 transitions of the *trans* isomer.<sup>28</sup> They made the additional argument that the most sterically stable form of their 1-propanol precursor would favor the formation of *trans*-*n*-methylvinoxide. In the SEVI experiment, formation of the *n*-methylvinoxide anion from the 1-propanal precursor happens very early in the molecular expansion, while the sample gas is still partly confined by the walls of the discharge source. We thus expect that the relevant molecule to consider for this steric argument is the *n*-methylvinoxide anion, which is more stable in its *cis* form (see Table IV). While Alconcel *et al.* reproduce the broad envelope of the PES data assuming a majority of *trans* isomer, SEVI is able to “zoom-in” on the spectrum revealing transitions that were previously not resolved. In particular, we have resolved peaks B through E in the binding energy region of 1.6 and 1.7 eV.

The locations and intensities of these peaks do not match Alconcel's *trans* simulations and in fact appear to match their *cis* simulations better (if the *cis* origin is translated). The SEVI spectra presented here also reveal the presence of peak Z due to the  $\tilde{X}^1A'$  state *trans* origin. This low intensity peak (only 10% as intense as peak A) was hidden underneath the broad low-energy tail of the main peak in the PES data.

## VII. CONCLUSIONS

The  $\tilde{X}^2A'' \leftarrow \tilde{X}^1A'$  and  $\tilde{A}^2A' \leftarrow \tilde{X}^1A'$  SEVI spectra of the *n*-methylvinoxide anion and its deuterated isotopologue are reported. Comparisons with FC simulations indicate that the majority of the spectral features are due to the *cis* isomer, while the higher-energy *trans* isomer contributes only a small origin peak, contrary to previous conclusions. A new value for the EA of *cis-n*-C<sub>3</sub>H<sub>5</sub>O has thus been determined at  $1.6106 \pm 0.0008$  eV with an associated  $\tilde{A}$  state term energy of  $1.167 \pm 0.002$  eV, while the EA of *trans-n*-C<sub>3</sub>H<sub>5</sub>O is  $1.570 \pm 0.002$  eV and the term energy is the same at  $1.167 \pm 0.003$  eV. For the first time, individual vibrational modes in the  $\tilde{X}^2A''$  and  $\tilde{A}^2A'$  states of *n*-methylvinoxy have been identified. A combination of anisotropy and frequency information reveal that the *n*-methylvinoxy SEVI spectra also display transitions that are only allowed through vibronic coupling between the  $\tilde{X}^2A''$  and  $\tilde{A}^2A'$  radical states.

## ACKNOWLEDGMENTS

This work was supported by the Air Force Office of Scientific Research (USAFOSR) under Grant No.'s F49620-03-1-0085 and FA9550-09-1-0343. We thank Dr. Gabriel M. P. Just for help with the excited state calculations. T.I.Y. thanks the Fonds québécois de la recherche sur la nature et les technologies (FQRNT) for a master's scholarship. T.I.Y. and E.G. thank the National Science and Engineering Research Council of Canada (NSERC) for post graduate scholarships.

- <sup>1</sup>K. M. Ervin, J. Ho, and W. C. Lineberger, *J. Phys. Chem.* **92**, 5405 (1988).
- <sup>2</sup>P. C. Engelking, G. B. Ellison, and W. C. Lineberger, *J. Chem. Phys.* **69**, 1826 (1978).
- <sup>3</sup>A. Sanov and R. Mabbs, *Int. Rev. Phys. Chem.* **27**, 53 (2008).
- <sup>4</sup>D. M. Neumark, *J. Phys. Chem. A* **112**, 13287 (2008).
- <sup>5</sup>T. N. Kitsopoulos, I. M. Waller, J. G. Loeser, and D. M. Neumark, *Chem. Phys. Lett.* **159**, 300 (1989).
- <sup>6</sup>E. Garand, J. Zhou, D. E. Manolopoulos, M. H. Alexander, and D. M. Neumark, *Science* **319**, 72 (2008).
- <sup>7</sup>E. Garand, T. I. Yacovitch, J. Zhou, S. M. Sheehan, and D. M. Neumark, *Chem. Sci.* **1**, 192 (2010).
- <sup>8</sup>J. Zhou, E. Garand, W. Eisfeld, and D. M. Neumark, *J. Chem. Phys.* **127**, 034304 (2007).
- <sup>9</sup>T. I. Yacovitch, E. Garand, and D. M. Neumark, *J. Phys. Chem. A* **114**, 11091 (2010).

- <sup>10</sup>E. Garand, T. I. Yacovitch, and D. M. Neumark, *J. Chem. Phys.* **129**, 074312 (2008).
- <sup>11</sup>T. I. Yacovitch, E. Garand, and D. M. Neumark, *J. Chem. Phys.* **130**, 244309 (2009).
- <sup>12</sup>M. Hassouna, E. Delbos, P. Devolder, B. Viskolcz, and C. Fittschen, *J. Phys. Chem. A* **110**, 6667 (2006).
- <sup>13</sup>H. E. Hunziker, H. Knepe, and H. R. Wendt, *J. Photochem.* **17**, 377 (1981).
- <sup>14</sup>K. T. Kuwata, A. S. Hasson, R. V. Dickinson, E. B. Petersen, and L. C. Valin, *J. Phys. Chem. A* **109**, 2514 (2005).
- <sup>15</sup>P. Casavecchia, G. Capozza, E. Segoloni, F. Leonori, N. Balucani, and G. G. Volpi, *J. Phys. Chem. A* **109**, 3527 (2005).
- <sup>16</sup>T. Ichino, S. M. Villano, A. J. Gianola, D. J. Goebbert, L. Velarde, A. Sanov, S. J. Blanksby, X. Zhou, D. A. Hrovat, W. T. Borden, and W. C. Lineberger, *J. Phys. Chem. A* **115**, 1634 (2011).
- <sup>17</sup>P. S. Thomas, R. Chhantyal-Pun, N. D. Kline, and T. A. Miller, *J. Chem. Phys.* **132**, 114302 (2010).
- <sup>18</sup>M. S. Bowen and R. E. Continetti, *J. Phys. Chem. A* **108**, 7827 (2004).
- <sup>19</sup>L. S. Alconcel, H. J. Deyerl, V. Zengin, and R. E. Continetti, *J. Phys. Chem. A* **103**, 9190 (1999).
- <sup>20</sup>S. Williams, E. Zingher, and J. C. Weisshaar, *J. Phys. Chem. A* **102**, 2297 (1998).
- <sup>21</sup>D. L. Osborn, H. Choi, D. H. Mordaunt, R. T. Bise, D. M. Neumark, and C. M. Rohlfing, *J. Chem. Phys.* **106**, 3049 (1997).
- <sup>22</sup>L. R. Brock and E. A. Rohlfing, *J. Chem. Phys.* **106**, 10048 (1997).
- <sup>23</sup>Y. Endo, S. Shuji, and E. Hirota, *J. Chem. Phys.* **83**, 2026 (1985).
- <sup>24</sup>R. D. Mead, K. R. Lykke, W. C. Lineberger, J. Marks, and J. I. Brauman, *J. Chem. Phys.* **81**, 4883 (1984).
- <sup>25</sup>L. F. DiMauro, M. Heaven, and T. A. Miller, *J. Chem. Phys.* **81**, 2339 (1984).
- <sup>26</sup>G. B. Ellison, P. C. Engelking, and W. C. Lineberger, *J. Phys. Chem.* **86**, 4873 (1982).
- <sup>27</sup>M. Baldi, F. Milella, G. Ramis, V. S. Escribano, and G. Busca, *Appl. Catal. A* **166**, 75 (1998).
- <sup>28</sup>L. S. Alconcel, H. J. Deyerl, and R. E. Continetti, *J. Am. Chem. Soc.* **123**, 12675 (2001).
- <sup>29</sup>B. C. Römer and J. I. Brauman, *J. Am. Chem. Soc.* **119**, 2054 (1997).
- <sup>30</sup>E. A. Brinkman, S. Berger, J. Marks, and J. I. Brauman, *J. Chem. Phys.* **99**, 7586 (1993).
- <sup>31</sup>A. H. Zimmerman, K. J. Reed, and J. I. Brauman, *J. Am. Chem. Soc.* **99**, 7203 (1977).
- <sup>32</sup>S. Williams, L. B. Harding, J. F. Stanton, and J. C. Weisshaar, *J. Phys. Chem. A* **104**, 9906 (2000).
- <sup>33</sup>A. Osterwalder, M. J. Nee, J. Zhou, and D. M. Neumark, *J. Chem. Phys.* **121**, 6317 (2004).
- <sup>34</sup>A. Eppink and D. H. Parker, *Rev. Sci. Instrum.* **68**, 3477 (1997).
- <sup>35</sup>E. J. Corey and J. W. Suggs, *Tetrahedron Lett.* **16**, 2647 (1975).
- <sup>36</sup>U. Even, J. Jortner, D. Noy, N. Lavie, and C. Cossart-Magos, *J. Chem. Phys.* **112**, 8068 (2000).
- <sup>37</sup>E. Garand, T. I. Yacovitch, and D. M. Neumark, *J. Chem. Phys.* **130**, 064304 (2009).
- <sup>38</sup>W. C. Wiley and I. H. McLaren, *Rev. Sci. Instrum.* **26**, 1150 (1955).
- <sup>39</sup>D. W. Chandler and P. L. Houston, *J. Chem. Phys.* **87**, 1445 (1987).
- <sup>40</sup>E. W. Hansen and P.-L. Law, *J. Opt. Soc. Am. A* **2**, 510 (1985).
- <sup>41</sup>K. L. Reid, *Annu. Rev. Phys. Chem.* **54**, 397 (2003).
- <sup>42</sup>J. Cooper and R. N. Zare, *J. Chem. Phys.* **48**, 942 (1968).
- <sup>43</sup>E. P. Wigner, *Phys. Rev.* **73**, 1002 (1948).
- <sup>44</sup>M. P. Andersson and P. Uvdal, *J. Phys. Chem. A* **109**, 2937 (2005).
- <sup>45</sup>M. J. Frisch, G. W. Trucks, H. B. Schlegel *et al.*, GAUSSIAN 03, Revision C.02, Gaussian, Inc., Wallingford CT, 2004.
- <sup>46</sup>F. Duschinsky, *Acta Physicochim. U.R.S.S.* **7**, 551 (1937).
- <sup>47</sup>K. M. Ervin, FCGAUSS03: GAUSSIAN 03 Output Conversion Program (2009).
- <sup>48</sup>K. M. Ervin, PESCAL, FORTRAN program (2009).
- <sup>49</sup>K. R. Asmis, T. R. Taylor, and D. M. Neumark, *J. Chem. Phys.* **111**, 8838 (1999).
- <sup>50</sup>K. M. Ervin and W. C. Lineberger, *J. Phys. Chem.* **95**, 1167 (1991).